IEEE Access
Multidisciplinary | Rapid Review | Open Access Journal

Received August 29, 2021, accepted September 24, 2021, date of publication September 29, 2021, date of current version October 8, 2021.

*Digital Object Identifier 10.1109/ACCESS.2021.3116247*

# A Novel Conductivity Classification Technique for Nonmagnetic Metal Immune to Tilt Variations Using Eddy Current Testing

**YUSHAN LIU[1], ZHIJIE ZHANG[1], (Member, IEEE), WULIANG YIN[1,2], (Senior Member, IEEE), HAOZE CHEN[1], ZHENGHUI YU[1], AND QUAN WANG[1]**

[1]School of Instrument and Electronics, North University of China, Taiyuan 030051, China
[2]School of Electrical and Electronic Engineering, The University of Manchester, Manchester M13 9PL, U.K.

Corresponding author: Zhijie Zhang (zhangzhijie@nuc.edu.cn)

This work was supported by the Fund for Shanxi 1331 Project Key Subject Construction of China.

**ABSTRACT** The widespread promotion of the concept of circular economy has placed higher demands on the sorting and recycling of metals. Eddy current testing as a non-contact, economical and fast response non-destructive testing technology provides a new development direction for the laborious task of classifying non-magnetic metal. The inevitable inclined surfaces in the metal classification process increase the difficulty of classification. In this paper, we present a novel conductivity classification technique for nonmagnetic metal, which uses the method of minimum error of characteristic slope to identify the metal property. The characteristic slope is extracted by fitting the line obtained from the endpoint of the maximum magnitude of mutual inductance trajectory under different tilt angles. The characteristic slope exists due to the consistency of the phase of the magnitude peak endpoints The test results show that the technique performs accurately in classifying five non-magnetic metals, copper, aluminum, zinc, tin, and titanium, within the tilt angle of 16.7°, and the technique still has good classification performance when the tilt angle is extended to 45°. This method benefits to achieve real-time metal classification.

**INDEX TERMS** Conductivity classification, characteristic slope, eddy current testing, nonmagnetic metal, tilt.

## I. INTRODUCTION

In recent years, the circular economy (CE) requires to improve the utilization efficiency of resources and reduce environmental costs while pursuing the maximum economic and social benefits. The concept aims to optimize material use by reusing, remanufacturing and recycling products to solve the problem of resource shortage [1]. The automobile manufacturing industry is one of the industries that consume a large amount of metal resources [2], thus the end-of-life vehicles (ELVs) contain a large amount of metal resources. End-of-life vehicle recycling processes is a combination of the removal of pollutants, automotive shredding and the classification of residue [3], [4]. The recovery of valuable metal materials from automotive shredder residues (ASR) is one of the key steps in ELV recycling, which mainly includes ferrous metal and non-ferrous metal sorting [5]. The efficiencies for ELV recycling processes are based on the processing efficiencies of magnetic separation, eddy current separation, heavy media separation, and other relevant processes used to retrieve valuable materials [1].

A crucial step towards metal classification for recycling is the development of real-time, non-contact classification methods to enable identification of category differences in metals on the conveyor belt. In this respect, nonmagnetic metals cannot be classified during the recovery process using magnetic deflection forces like ferromagnetic metals [6], but different types of nonmagnetic metals have different conductive properties. Therefore, eddy current testing is very suitable for detecting the electromagnetic properties of metals due to the advantages of non-contact, non-destructive, high adaptability, and fast detection speed [7]–[9]. Currently, there are three main techniques for eddy current testing: single-frequency eddy current (SEC) testing, multifrequency eddy current (MEC) testing, and pulsed eddy current (PEC) testing [10]–[15]. Among them, SEC and PEC have a fast

The associate editor coordinating the review of this manuscript and approving it for publication was Xiaokang Yin.

response compared to MEC and can be used for online measurements [16], [17]. Recently, eddy current testing is widely used in metal electromagnetic property inspection [18]–[22]. Cuiping Wang *et al.* obtained a log-linear relationship between impedance phase and conductivity by measuring the variation of impedance values at a point above the center of copper, brass and four alloys of aluminum samples [23]. However, this method only measured the variation above the center of the sample and did not take into account the randomness of metal placement such as tilting angle. Yue Du *et al.* proposed a method to classify five nonferrous metal samples with a tilt angle no greater than 9° using the characteristic phase of the mutual inductance trajectory combined with a photoelectric sensor [24], but the introduction of the photoelectric sensor also introduced fitting errors.

In this paper, we propose a new method based on the characteristic slope of the peak endpoint of the magnitude of the mutual inductance trajectory. The method using single-frequency eddy current testing at an excitation frequency of 60KHz achieves the classification of five nonmagnetic metal samples within a tilt angle of 16.93° using only an eddy current sensor without auxiliary settings, which is larger than the previous 9° in [24]. The analytical solution of the mutual inductance for the eddy current sensor above metal plate is given in Section II. In Section III, we present the experimental setup by which we can obtain the mutual inductance trajectory of the dynamic scanning process of the eddy current probe with respect to the metal sample. In Section IV, we find the characteristic slopes of five metals with different conductivities extracted from the mutual inductance trajectories of metals with different tilt angles. Based on the above characteristic slopes, we propose a minimum error-based classification technique and test it in Section V. We discuss the explanation for the existence of the characteristic slope in Section VI. The experimental results demonstrate that the novel technique can successfully classify five nonmagnetic metals within a tilt angle of 16.93°.

## II. THEORETICAL FOUNDATION

Since Dodd and Deeds in [25] obtained analytical solutions to eddy current probe coil problems given in the following equations, analytical solutions have been widely used in eddy current problems.

$$\Delta L(\omega) = K \int_0^{\infty} \frac{P^2(\alpha)}{\alpha^6} A(\alpha)\phi(\alpha)d\alpha \tag{1}$$

$$K = \frac{\pi \mu_0 N^2}{(l_1 - l_2)^2 (r_1 - r_2)^2} \tag{2}$$

$$P(\alpha) = \int_{\alpha r_1}^{\alpha r_2} xJ_1(x)dx \tag{3}$$

$$A(\alpha) = \left(e^{-\alpha l_1} - e^{-\alpha l_2}\right)^2 \tag{4}$$

$$\phi(\alpha) = \frac{(\alpha_1 + \alpha)(\alpha_1 - \alpha) - (\alpha_1 + \alpha)(\alpha_1 - \alpha)e^{2\alpha_1 c}}{-(\alpha_1 - \alpha)(\alpha_1 - \alpha) + (\alpha_1 + \alpha)(\alpha_1 + \alpha)e^{2\alpha_1 c}} \tag{5}$$

$$\alpha_1 = \sqrt{\alpha^2 + j\omega\sigma\mu_0} \tag{6}$$

where $\mu_0$ denotes the permeability of free space, $N$ is the number of coil turns, $r_1$ and $r_2$ is the inner and outer radius of the coil, $l_1$ is the lift-off, $l_2 - l_1$ is the coil height, $c$ is the plate thickness, $\sigma$ is the conductivity, $\omega$ is the excitation angular frequency, $\alpha$ is the spatial frequency.

The mutual inductance $\Delta L$ can be expressed in the form of magnitude and phase, as in (7)-(9).

$$\Delta L_r + i\Delta L_i = |\Delta L|e^{j\theta} \tag{7}$$

$$|\Delta L| = \sqrt{\Delta L_r^2 + \Delta L_i^2} \tag{8}$$

$$\theta = \arctan\left|\frac{\Delta L_i}{\Delta L_r}\right| \tag{9}$$

where $\Delta L_r$ is the real part of $\Delta L$, $\Delta L_i$ is the imaginary part of $\Delta L$, $|\Delta L|$ is the magnitude of $\Delta L$, $\theta$ is the phase of $\Delta L$.

Based on the fact that $\phi(\alpha)$ changes slowly with $\alpha$ [26], (1) can be approximated as

$$\Delta L(\omega) = \phi(\alpha_0)\,\Delta L_0 \tag{10}$$

where

$$\phi(\alpha_0) = \frac{(\alpha_1+\mu\alpha_0)(\alpha_1-\mu\alpha_0)-(\alpha_1+\mu\alpha_0)(\alpha_1-\mu\alpha_0)e^{2\alpha_1 c}}{-(\alpha_1-\mu\alpha_0)(\alpha_1-\mu\alpha_0)+(\alpha_1+\mu\alpha_0)(\alpha_1+\mu\alpha_0)e^{2\alpha_1 c}} \tag{11}$$

$$\Delta L_0 = K \int \frac{P^2(\alpha)}{\alpha^6} A(\alpha)d\alpha \tag{12}$$

According to (10), the phase of the eddy current sensor is related to the conductivity, and plate thickness, and are approximately independent of the lift-off height. L is the magnitude of the sensor signal, which is very dependent on the lifting distance. The magnitude decreases with the increase of lifting height.

## III. EXPERIMENTAL SET-UP

We select five non-magnetic metal samples with different conductivity of copper, aluminum, zinc, tin, and titanium as shown in Table 1. The sample size is 1cm × 1cm × 1cm in the experiment. The sensor consists of two coils of the same size, one as excitation and the other as receiver. As shown in Fig. 1, the excitation and receiver coils are placed parallel to each other above the sample, and the geometric dimensions of the sensor are shown in Table 2. The experimental setup is shown in Fig. 2. The Zurich impedance analyzer is used to measure the mutual impedance change between the excitation coil and the receiving coil of the eddy current sensor, and the PC is connected to the impedance analyzer for setting the excitation signal parameters and receiving the data. We change the tilt angle by placing spacers on the bottom side of the sample in Fig. 2. The transformation of mutual inductance and impedance is given by

$$\mathrm{Re}(\Delta L) = \mathrm{Re}\left(\frac{Z_s - Z_a}{j\omega}\right) \tag{13}$$

$$\mathrm{Im}(\Delta L) = \mathrm{Im}\left(\frac{Z_s - Z_a}{j\omega}\right) \tag{14}$$

**TABLE 1. Conductivity of the metals.**

| Metal | Conductivity (MS/m) |
|---|---|
| Titanium | 2.40 |
| Tin | 9.20 |
| Zinc | 16.9 |
| Aluminum | 37.7 |
| Copper | 59.6 |

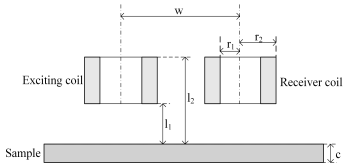


**FIGURE 1. Schematic diagram of eddy current testing principle.**

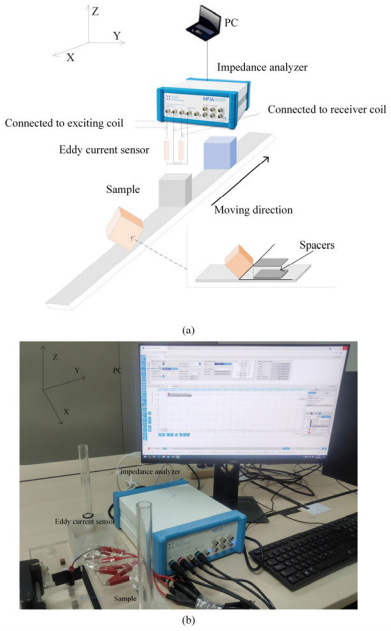


**FIGURE 2. Experimental setup (a) schematic diagram (b) actual setup.**

where $Z_s$ is the impedance of the coil above the sample, $Z_a$ is the impedance of the coil in free space $\omega$ is the angular frequency of the excitation signal, $\Delta L$ is the change of mutual inductance. By using the inductance variation equation in (13) and (14), the ambient noise signal is excluded from the experimental inductance variation to obtain the value of the mutual inductance variation from the sample.

The experimental procedure consists mainly of non-tilted as well as tilted metal samples of different angles moving along the Y-axis with the eddy current probe fixed. The tilt angle is changed by adding spacer to the side under the sample. The PC records the mutual impedance changes of this dynamic process by means of the impedance analyzer.

## IV. EXTRACTION OF FEATURE

Fig. 3 and Fig. 4 show the mutual inductance trajectories obtained from the above experimental setup in the form of real and imaginary parts at 60 KHz excitation frequency when

**TABLE 2. Sensor parameters.**

| Coil parameters | Value |
|---|---|
| Inner radius of the excitation/receiving coil ($r_1$) | 0.98mm |
| Outer radius of the excitation/receiving coil (r2) | 1.5mm |
| The lift-off (l1) | 5mm |
| Hight of the excitation/receiving coil (l2-l1) | 1.6mm |
| Center distance between two coils (w) | 4.5mm |
| Number of turns (N) | 100 |

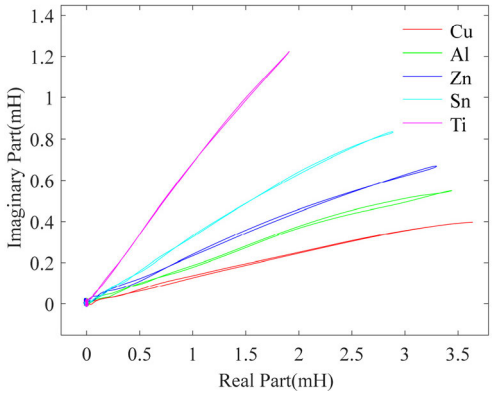


**FIGURE 3. Mutual inductance trajectory at 60KHz excitation frequency of five metals at an inclination angle of 0°.**

the eddy current probe scans the non-tilted and tilted samples according to a certain path. The mutual inductance trajectory is a petal-shaped multi-valued curve, which is because the sample is an away-near-away process relative to the eddy current probe during the scanning process. When the tilt angle is 0, the lift-off is 5 mm, and the subsequent tilt samples remain unchanged. The trajectories of the mutual inductance values of the different types of samples are distinguished from each other and rotate clockwise from titanium to copper with increasing conductivity. With the gradual increase of the tilt angle from 0, we can observe that the magnitude of mutual inductance increases, which is because the increase of the tilt angle causes the highest point of the sample from the lower edge of the sensor to reduce the lift-off, which causes the eddy current strength to increase, resulting in the increase of the probe mutual inductance.

Although the mutual inductance trajectories of the five samples were separated from each other at the determined angles, we did not find the characteristic quantities that could characterize the metal properties at different tilt angles. To solve the tilt angle problem, we first combined the trajectories of the same sample at different tilt angles in one plot, as shown in Fig. 5. The length and width of the petal shape curve increase with increasing tilt angle, which is due to the increased asymmetry of the scan plane below the eddy current probe. We find that for the same sample, the mutual inductance trajectories with different tilt angles are roughly on the same straight line at the endpoint of the maximum magnitude. Denote these endpoints as $(x_{ij}, y_{ij})i = 1 - 5$, successively denoting five metals of copper, aluminum, zinc, tin and titanium, j =1-7, respectively denoting tilt

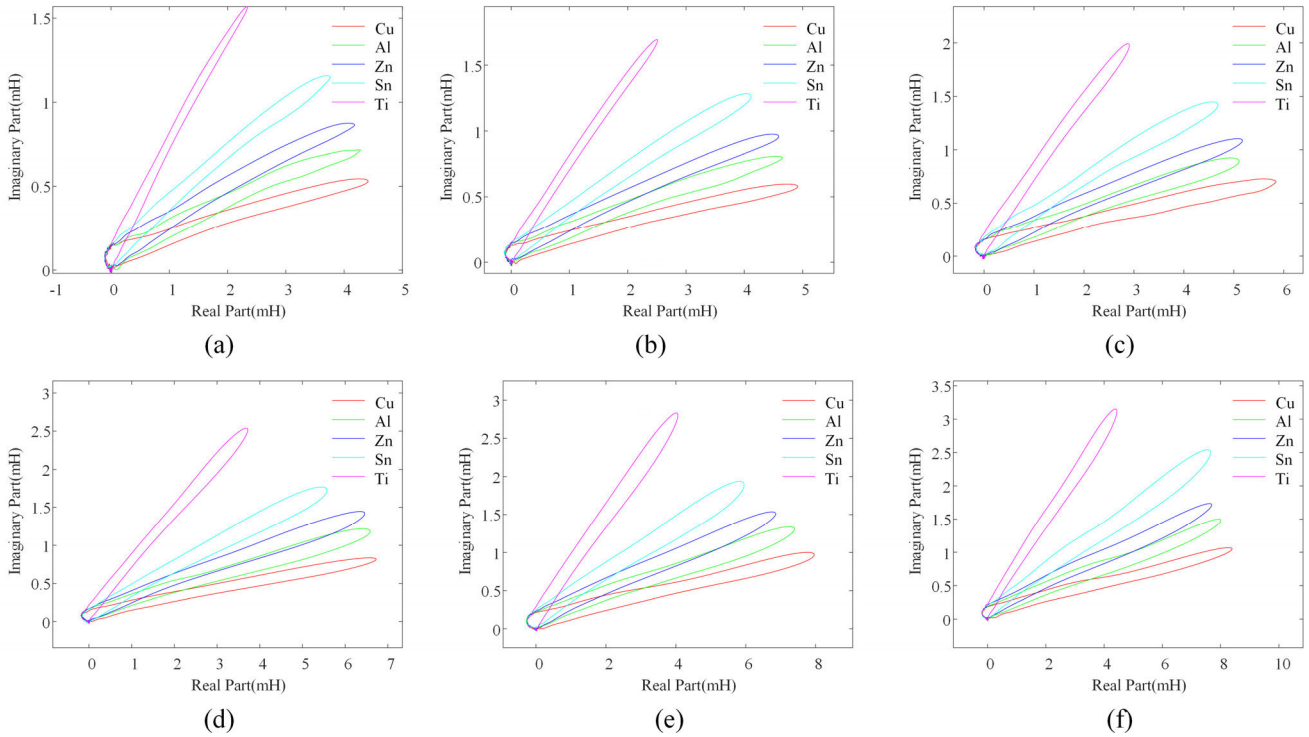


**FIGURE 4.** Mutual inductance trajectory at 60KHz excitation frequency of five metals in the tilt angle of (a) 3.8° (b) 5.7° (c) 7.6° (d)11.3° (e) 14.9° (f) 16.7°.

**TABLE 3.** Characteristic slope extracted from mutual inductance trajectory of the five metals.

| Metal | Characteristic slope |
|---|---|
| Titanium | 0.7397 |
| Tin | 0.3479 |
| Zinc | 0.2410 |
| Aluminum | 0.1992 |
| Copper | 0.1327 |

angles 0°, 3.8°, 5.7°, 7.6°, 11.3°, 14.9° and 16.7°. By fitting these endpoints with the least square method, a straight line with a determined slope and intercept is obtained. The least squares fitting method is given by

$$y_{ij} = k_i x_{ij} + b_i \tag{15}$$

$$k_i = \frac{\overline{x_{ij}y_{ij}} - \overline{x_{ij}}\,\overline{y_{ij}}}{\overline{x_{ij}^2} - \overline{x_{ij}}^2} \tag{16}$$

$$b_i = \overline{y_{ij}} - k_i\overline{x_{ij}} \tag{17}$$

where $k_i$ and $b_i$ is slope and intercept of the fitting line.

Fig. 6 shows that the slope of the fitting line decreases with the increase of conductivity, which is consistent with the fact that the mutual inductance trajectory rotates clockwise with increasing conductivity in the first quadrant of the Cartesian coordinate system. For each metal sample, we obtain a point set as well as a slope set as shown in Tables 3 and Table 4.

According to Table 3, the slopes of the fitted straight lines obtained for different samples can be used as feature quantities to distinguish nonmagnetic metal samples with different conductivities. To investigate the reason for the existence of the characteristic slope, we calculated the phase of the magnitude peak endpoints listed in Table 4 according to (14) in Section III. The results are shown in Fig. 7. We found that the phase of the peak magnitude endpoints of the same metal is almost independent of the tilt angle. This agrees with the conclusion of (8) in Section II, because the sample thickness is much larger than the skinning depth, and we consider that the tilt can be approximated as an increase in the lift-off.

## V. CONDUCTIVITY CLASSIFICATION TECHNIQUE AND TEST

Based on the slope set and point set of the above five metal samples, this paper proposes a novel technique for classifying the conductivity of tilted nonmagnetic metal samples in accordance with the minimum error of characteristic slope. The steps are as follows.

1) Slide the metal sample of unknown angle and type and measure the raw data of mutual inductance change L by the experimental system
2) Find the point $(x_0, y_0)$ of the maximum magnitude of the mutual inductance complex plane.
3) The point $(x_0, y_0)$ is respectively fitted with the preceding 5 point sets by least squares to obtain 5 straight lines. $s_i$ denotes the slope of the line.
4) The slope $s_i$ of five straight lines is compared with the characteristic slope $k_i$ of five metals, and the metal corresponding to the line with the smallest difference is the classification result.

$$[i, \delta] = \min |s_i - k_i| \tag{18}$$

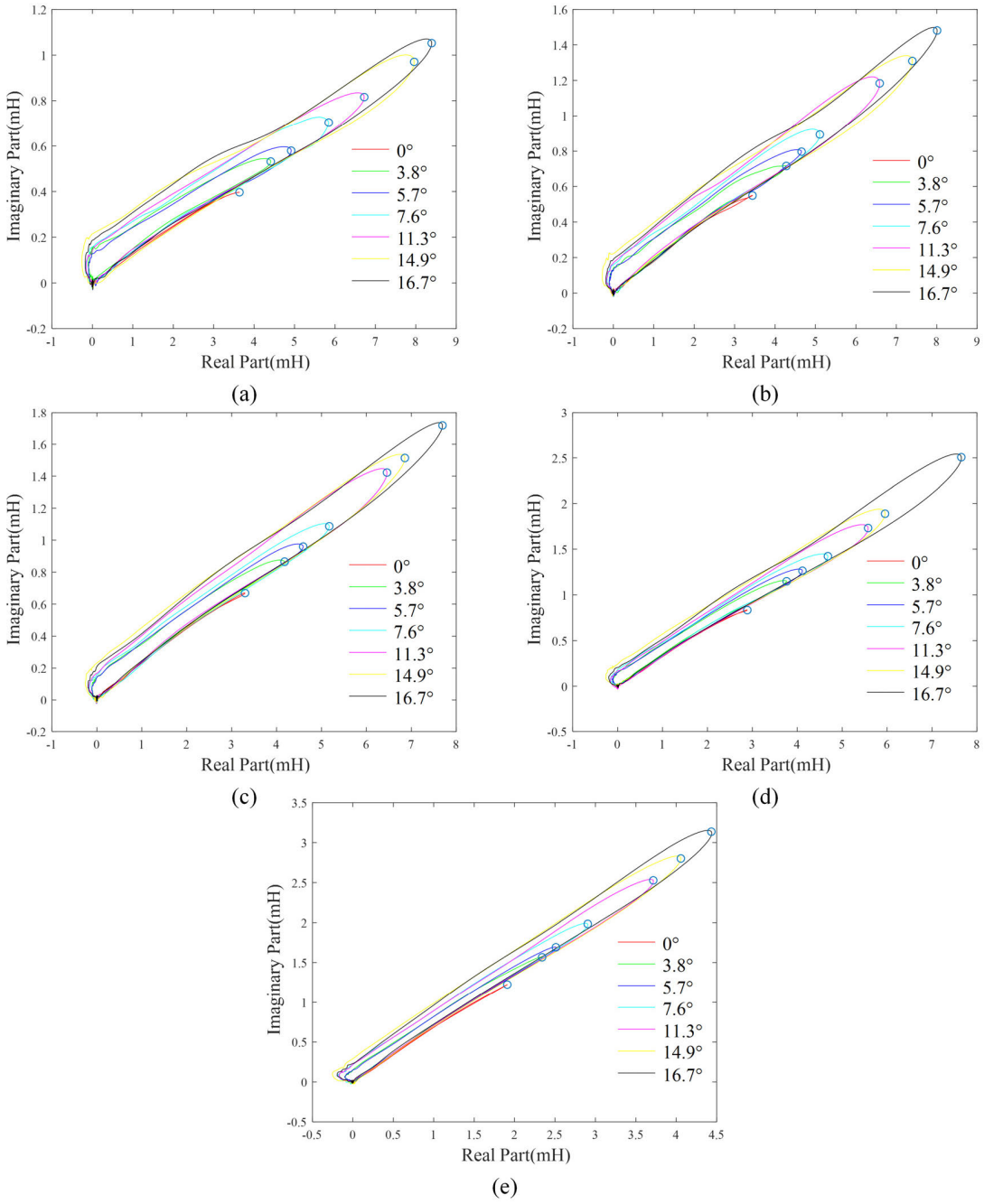


**FIGURE 5.** Mutual inductance trajectory under different tilt angles of (a) copper (b) aluminum (c) zinc (d) tin (e) titanium, the endpoints of the magnitude peaks marked by circles are approximately distributed on a straight line.

**TABLE 4.** The peak magnitude endpoint of the mutual inductance trajectory of the five metals.

| Metal | Titanium | Tin | Zinc | Aluminum | Copper |
|---|---|---|---|---|---|
| 0° | (1.910, 1.223) | (2.887, 0.8342) | (3.297, 0.6695) | (3.442, 0.5495) | (3.638, 0.3968) |
| 3.8° | (2.341, 1.566) | (3.763, 1.150) | (4.178, 0.8654) | (4.278, 0.7157) | (4.411, 0.5318) |
| 5.7° | (2.511, 1.691) | (4.116, 1.265) | (4.592, 0.9597) | (4.656, 0.7966) | (4.916, 0.5795) |
| 7.6° | (2.905, 1.983) | (4.682, 1.423) | (5.174, 1.087) | (5.108, 0.8937) | (5.846, 0.7035) |
| 11.3° | (3.716, 2.528) | (5.577, 1.732) | (6.458, 1.423) | (5.589, 1.184) | (6.724, 0.8158) |
| 14.9° | (4.057, 2.803) | (5.954, 1.889) | (6.856, 1.514) | (7.397, 1.310) | (7.959, 0.9707) |
| 16.7° | (4.434, 3.136) | (7.652, 2.508) | (7.694, 1.718) | (8.009, 1.481) | (8.392, 1.052) |

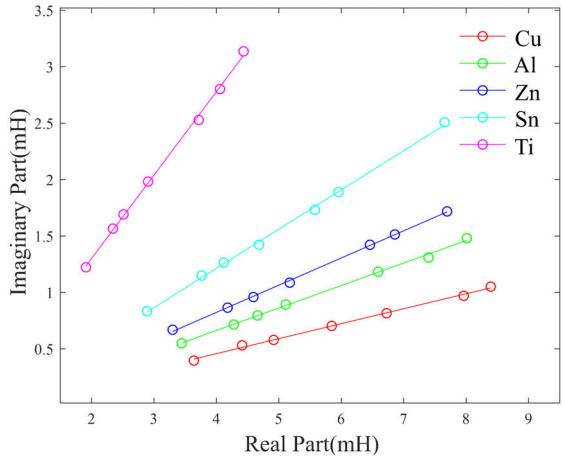


**FIGURE 6.** Fitting line of five metals extracted from the mutual inductance trajectory, the circles mark the peak magnitude endpoints.

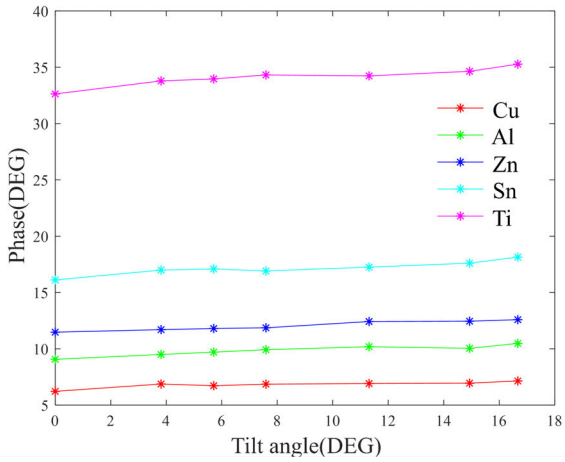


**FIGURE 7.** The phase corresponding to the peak magnitude endpoint of five metals.

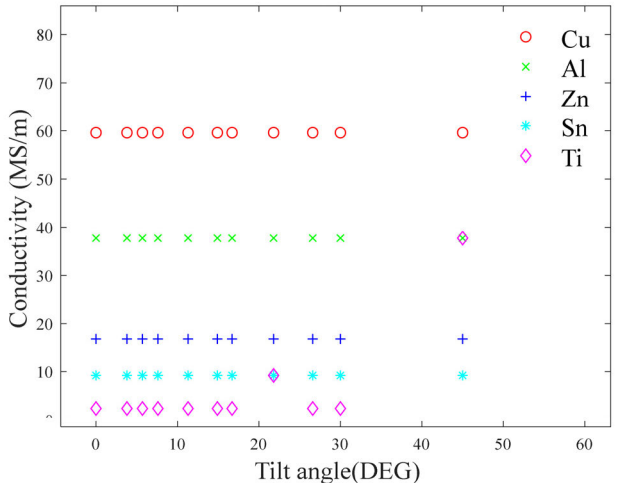


**FIGURE 8.** Test results of the technique, titanium misclassified as tin at an inclination angle of 21.8° as aluminum at an inclination angle of 21.8°.

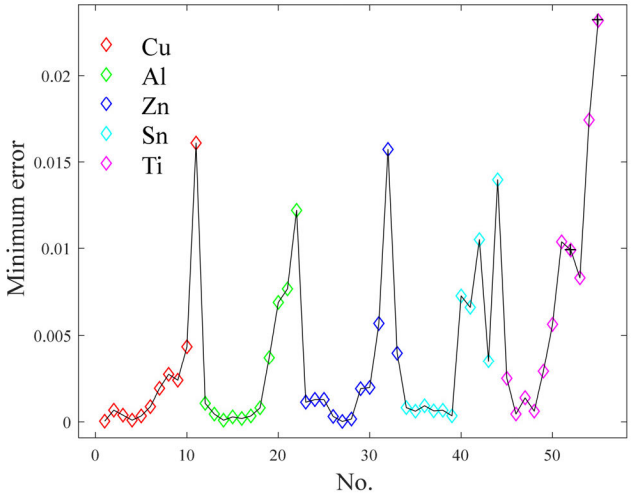


**FIGURE 9.** Minimum error corresponding to 55 sets of test data for 5 metals, in order of increasing tilt angle.

where i still denotes to the metal type, and $\delta$ is the minimum error.

To verify the feasibility of the method, we collected data from 55 groups of samples at different tilt angles as a test set for validation. Thirty-five of these data sets were within the tilt angle of 16.7°, and 20 data sets had an angle greater than 16.7°. The maximum value of the selected tilt angle is 45°. The tilt angle of the test data taken was greater than the tilt angle of the data we sampled for extracting the feature slope. The test results show in Fig. 8. This technique we proposed can successfully classify five metals when the tilt angle is less than 16.7°, and when the angle is increased to 45°, the method is still reliable with a classification rate of 96.4%. At an angle of 21.8°, titanium was incorrectly classified as tin. Titanium was incorrectly classified as aluminum at an angle of 45°. The test results perform well at large tilt angles, demonstrating the robustness of our technique to changes in tilt angle.

We selected five sets of test data in Table 5 to present the fitted slope, the minimum error of the fitted slope and the characteristic slope, and the classification result and the minimum error in the classification process. We can discover that for each metal, there is always one error value that is significantly smaller than the remaining four values in the minimum error of fitted slope and characteristic slope, and this minimum error corresponds to the characteristic slope, which is the type of metal corresponding to the classification result. We indicate the minimum error for each metal in order of angular scale in Fig. 9. We find that most of the minimum error values are below 0.004, and most of the minimum errors greater than 0.004 correspond to data with a tilt angle greater than 16.7°. Those marked with a cross are misclassification results. This indicates that the classification effect is weakened and the gap between the fitted slope and the characteristic slope is increased in the case of increasing degree.

## VI. DISCUSSION

To further investigate the existence of the characteristic slope, we tested the five metals in the non-tilt case at different lift-off, and the results are shown in Fig. 10. We found that the

**TABLE 5.** Fitting slope, error, and minimum error for 5 sets of test data in the classification process.

| Test metal | Tilt angle | $s_i$ | $\lvert s_i - k_i \rvert$ | $[i, \delta]$ |
|---|---|---|---|---|
| Titanium | 21.8° | (0.1630, 0.2855, 0.3628, 0.5072, 0.7473) | (0.03027, 0.08627, 0.1218, 0.1594, 0.008311) | (5, 0.008311) |
| Tin | 26.6° | (0.2970, 0.3258, 0.3383, 0.3366, 0.2172) | (0.1643, 0.1266, 0.09736, 0.01128, 0.5217) | (4, 0.01128) |
| Zinc | 16..7° | (0.1906, 0.2269, 0.2391, 0.2537, 0.09465) | (0.05793, 0.02774, 0.001898, 0.09420, 0.6443) | (3, 0.001898) |
| Aluminum | 11.3° | (0.1405, 0.1994, 0.2270, 0.2778, 0.07813) | (0.007848, 0.0001965, 0.01401, 0.07007, 0.6608) | (2, 0.0001965) |
| Copper | 5.7° | (0.1323, 0.2091, 0.2571, 0.3543, 0.2139) | (0.0003892, 0.009913, 0.01616, 0.006473, 0.5250) | (1, 0.0003892) |

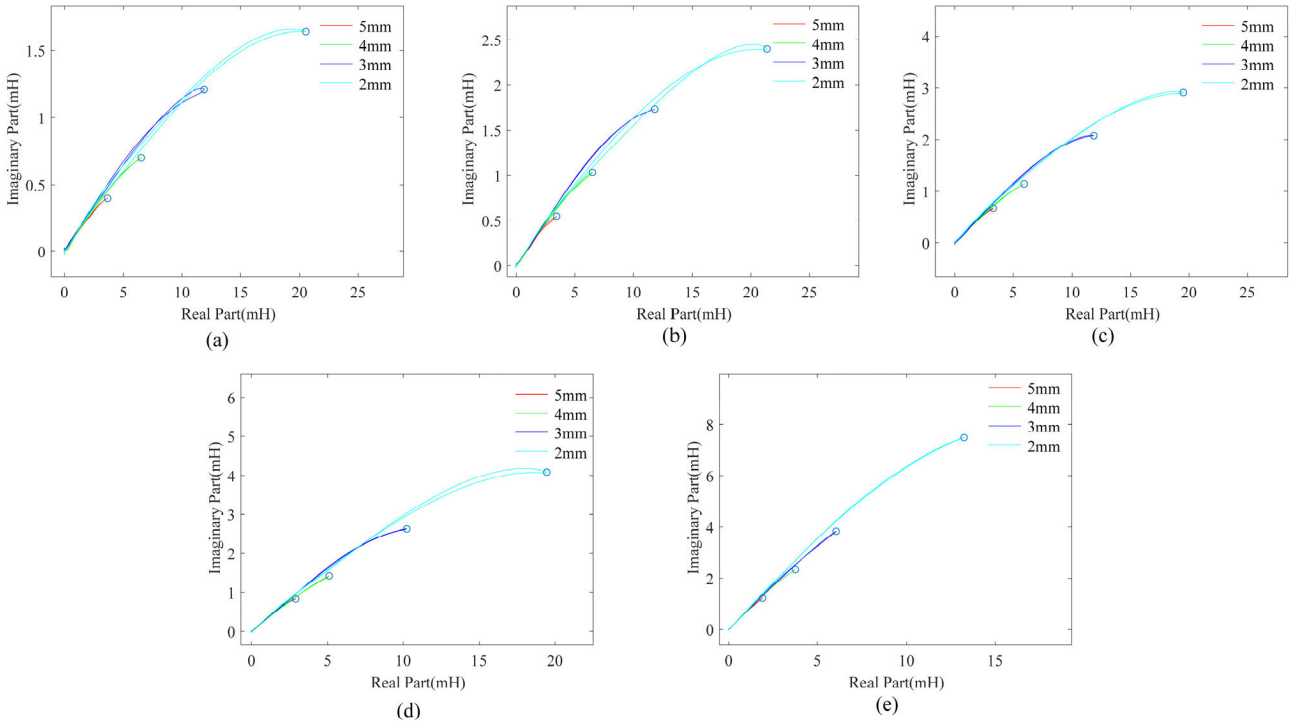


**FIGURE 10.** Mutual inductance trajectory under different lift-off of (a) copper (b) aluminum (c) zinc (d) tin (e) titanium, the circles mark the peak magnitude endpoints.

**TABLE 6.** Slopes extracted from the mutual inductance trajectories of the different lift-off of the five metals.

| Metal | Characteristic slope |
|---|---|
| Titanium | 0.5480 |
| Tin | 0.1939 |
| Zinc | 0.1378 |
| Aluminum | 0.1010 |
| Copper | 0.07300 |

magnitude is increasing as the lift-off decreases, which is consistent with the increasing tilt angle, but the petals have an overall curvature and are narrower in the non-tilt case. We also select the endpoints of the magnitude maximum to fit them as a straight line and calculate the phase values of these points in Fig. 11 and Fig. 12. The slopes of the fitted straight lines are shown in Table 6.

Comparing the data in Table 6 with those in Table 3, we find that the slope values of the fitted lines obtained from the lift-off variation decrease compared to the tilt variation, which is consistent with the fact that the lift-off fitted lines are rotated clockwise with respect to the tilt fitted lines found

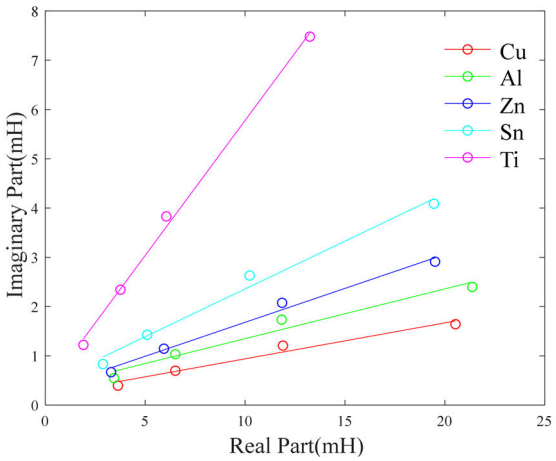


**FIGURE 11.** Fitting line of five metals extracted from the mutual inductance trajectory under different lift-off, the circles mark the peak magnitude endpoints.

in Fig. 11 compared with Fig. 6. The phase of the endpoints of the magnitude maxima of the mutual inductance trajectory obtained from the lift-off variation is also consistent

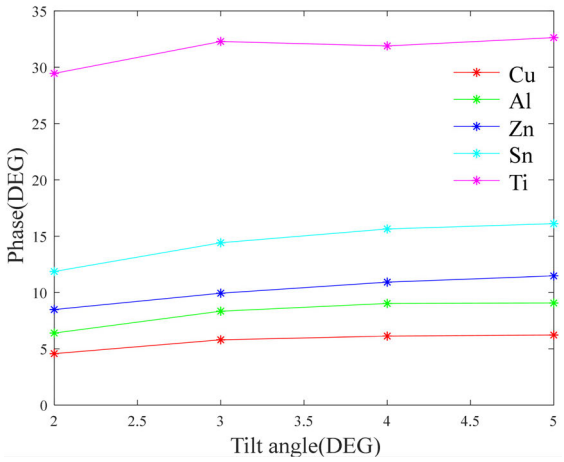


**FIGURE 12.** **The phase corresponding to the peak magnitude endpoint of five metals under different lift-off.**

in Fig. 12 corresponding to Fig. 7. Although the phase values change, i.e., they all decrease to some extent. This is attributed to the fact that the tilt, while reducing the lift-off height, also creates an asymmetric scan plane. However, the above analysis still demonstrates that the characteristic slope exists to a large extent due to the approximate independence of the phase from the lift-off height.

Although there have been studies of non-ferrous metal classification of tilted samples, one uses photoelectric sensors to compensate for errors caused by tilt angle [24], and the other uses the path of lift-off changes as the scan path of the eddy current probe [21]. However, the former one has a limited application of angle, achieving better classification only up to 9°. The latter one extends the inclination angle to 11.3° but brings inconvenience to the practical application. In this paper, we take the same experimental approach as in [24], without using photoelectric sensors, and select the slope as the classification feature value. The selection of robust feature values is significant to improve the classification accuracy. The test results in Section V. verify the reliability of the proposed classification technique. It is noteworthy that 36% of the data we tested had a tilt angle greater than 16.7° and still achieved a classification rate of 96.4%. In addition, the tilt angle of the data selected for our extracted features is less than 16.7°, which shows the stability of the slope of our extracted features. In the process of metal classification, there are still many problems to be solved, such as more types including alloys, and the lift-off effect prevalent in eddy current detection. In the next step of our research, we will work on solving the problem of both lift-off and angle change

## VII. CONCLUSION

In this paper, five kinds of non-magnetic metals are classified according to the minimum error of characteristic slope of mutual inductance. The characteristic slope is obtained by fitting a straight line from the peak points of the mutual inductance trajectory magnitude at different tilt angles. We found that the mutual inductance trajectories of the five metals scanned by path at 60 KHz excitation frequency rotate clockwise with increasing conductivity from titanium to copper in the first quadrant of the Cartesian coordinate system, and the magnitude of the trajectories increases with increasing tilt angle. In order to find the characteristic quantity that indicates the metal property at different tilt angles, we fit the peak points of the mutual inductance trajectory magnitude of the same metal at different tilt angles to a straight line based on the least square method, and on this basis, we propose a method to classify metals based on the minimum error of the characteristic slope. The test results exhibit that the technique can accurately classify five non-magnetic metals with tilt angles within 16.7°, and the accuracy can reach 96.4% when the tilt angle is extended to 45°. To explore the reason for the existence of the characteristic slope, we found that the phases of the selected magnitude peak points are consistent. The characteristic slope found in this paper may benefit to resolve the effect of the lift-off in the classification process. This classification system uses only eddy current sensors and single-frequency eddy current detection has a fast response time, which will help to realize an industrial system for real-time metal classification in the future.

## REFERENCES

[1] V. K. Soo, M. Doolan, P. Compston, J. R. Duflou, J. Peeters, and Y. Umeda, "The influence of end-of-life regulation on vehicle material circularity: A comparison of Europe, Japan, Australia and the US," *Resour., Conservation Recycling*, vol. 168, May 2021, Art. no. 105294.

[2] H. Ohno, K. Matsubae, K. Nakajima, Y. Kondo, S. Nakamura, and T. Nagasaka, "Toward the efficient recycling of alloying elements from end of life vehicle steel scrap," *Resour., Conservation Recycling*, vol. 100, pp. 11–20, Jul. 2015.

[3] V. K. Soo, J. Peeters, P. Compston, M. Doolan, and J. R. Duflou, "Comparative study of end-of-life vehicle recycling in Australia and Belgium," *Proc. CIRP*, vol. 61, pp. 269–274, Jan. 2017.

[4] A. Santini, L. Morselli, F. Passarini, I. Vassura, S. Di Carlo, and F. Bonino, "End-of-life vehicles management: Italian material and energy recovery efficiency," *Waste Manage.*, vol. 31, no. 3, pp. 489–494, Mar. 2011.

[5] F. Margarido, R. N. Santos, F. Durão, C. Guimarães, C. A. Nogueira, P. C. Oliveira, F. Pedrosa, and A. M. Gonçalves, "Separation of non-ferrous frations of shredded end-of-life vehicles for valorising its alloys," in *Proc. Int. Conf. Mining, Mater. Metall. Eng. (MMME)*, 2014, pp. 77-1–77-4.

[6] J. Oberteuffer, "Magnetic separation: A review of principles, devices, and applications," *IEEE Trans. Magn.*, vol. MAG-10, no. 2, pp. 223–238, Jun. 1974.

[7] R. Huang, M. Lu, A. Peyton, and W. Yin, "Thickness measurement of metallic plates with finite planar dimension using eddy current method," *IEEE Trans. Instrum. Meas.*, vol. 69, no. 10, pp. 8424–8431, Oct. 2020.

[8] R. Huang, M. Lu, X. He, A. Peyton, and W. Yin, "Measuring coaxial hole size of finite-size metallic disk based on a dual-constraint integration feature using multifrequency eddy current testing," *IEEE Trans. Instrum. Meas.*, vol. 70, pp. 1–7, 2021.

[9] M. Lu, X. Meng, R. Huang, L. Chen, A. Peyton, and W. Yin, "Inversion of distance and magnetic permeability based on material-independent and liftoff insensitive algorithms using eddy current sensor," *IEEE Trans. Instrum. Meas.*, vol. 70, pp. 1–9, 2021.

[10] X. Chen and Y. Lei, "Electrical conductivity measurement of ferromagnetic metallic materials using pulsed eddy current method," *NDT &E Int.*, vol. 75, pp. 33–38, Oct. 2015.

[11] A. V. Egorov, V. V. Polyakov, D. S. Salita, E. A. Kolubaev, S. G. Psakhie, A. G. Chernyavskii, and I. V. Vorobei, "Inspection of aluminum alloys by a multi-frequency eddy current method," *Defense Technol.*, vol. 11, no. 2, pp. 99–103, Jun. 2015.

[12] G. Tytko and L. Dziczkowski, "E-cored coil with a circular air gap inside the core column used in eddy current testing," *IEEE Trans. Magn.*, vol. 51, no. 9, pp. 1–4, Sep. 2015.

[13] W. Yin, R. Huang, M. Lu, Z. Zhang, and A. Peyton, "Measurements of thickness for metallic plates with co-axial holes using a novel analytical method with the modified integration range," *IEEE Access*, vol. 8, pp. 198301–198306, 2020.
[14] W. Yin and A. J. Peyton, "Thickness measurement of non-magnetic plates using multi-frequency eddy current sensors," *NDT &E Int.*, vol. 40, no. 1, pp. 43–48, Jan. 2007.
[15] F. Yuan, Y. Yu, L. Li, and G. Tian, "Investigation of DC electromagnetic-based motion induced eddy current on NDT for crack detection," *IEEE Sensors J.*, vol. 21, no. 6, pp. 7449–7457, Mar. 2021.
[16] S. Zhu, J. R. S. Avila, W. Yin, A. J. Peyton, J. Ding, and S. Williams, "Real-time measurement of electrical conductivity for aluminium wires using a novel calibration method," in *Proc. IEEE Int. Instrum. Meas. Technol. Conf. (IMTC)*, May 2020, pp. 1–5.
[17] Y. He, G. Y. Tian, H. Zhang, M. Alamin, A. Simm, and P. Jackson, "Steel corrosion characterization using pulsed eddy current systems," *IEEE Sensors J.*, vol. 12, no. 6, pp. 2113–2120, Jun. 2012.
[18] M. Lu, H. Xu, W. Zhu, L. Yin, Q. Zhao, A. Peyton, and W. Yin, "Conductivity lift-off invariance and measurement of permeability for ferrite metallic plates," *NDT &E Int.*, vol. 95, pp. 36–44, Apr. 2018.
[19] L. Dziczkowski, "Elimination of coil liftoff from eddy current measurements of conductivity," *IEEE Trans. Instrum. Meas.*, vol. 62, no. 12, pp. 3301–3307, Dec. 2013.
[20] S. Zhu, R. Huang, J. R. S. Avila, Y. Tao, Z. Zhang, Q. Zhao, A. J. Peyton, and W. Yin, "Simultaneous measurements of wire diameter and conductivity using a combined inductive and capacitive sensor," *IEEE Sensors J.*, vol. 20, no. 19, pp. 11617–11624, Oct. 2020.
[21] Y. Du, Z. Zhang, W. Yin, and G. Tytko, "Sloping-invariance for nonferrous metallic slabs at multiple frequencies by eddy current sensors," *IEEE Access*, vol. 9, pp. 59949–59956, 2021.
[22] W. Zhou, M. Lu, Z. Chen, L. Zhou, L. Yin, Q. Zhao, A. Peyton, Y. Li, and W. Yin, "Three-dimensional electromagnetic mixing models for dual-phase steel microstructures," *Appl. Sci.*, vol. 8, no. 4, p. 529, 2018.
[23] C. Wang, M. Fan, B. Cao, B. Ye, and W. Li, "Novel noncontact eddy current measurement of electrical conductivity," *IEEE Sensors J.*, vol. 18, no. 22, pp. 9352–9359, Nov. 2018.
[24] Y. Du, Z. Zhang, W. Yin, S. Zhu, Z. Chen, and H. Xu, "Conductivity classification of non-magnetic tilting metals by eddy current sensors," *Sensors*, vol. 20, no. 9, p. 2608, May 2020.
[25] C. Dodd and W. Deeds, "Analytical solutions to eddy-current probe-coil problems," *J. Appl. Phys.*, vol. 39, no. 6, pp. 2829–2838, 1968.
[26] W. Yin, R. Binns, S. J. Dickinson, C. Davis, and A. J. Peyton, "Analysis of the liftoff effect of phase spectra for eddy current sensors," *IEEE Trans. Instrum. Meas.*, vol. 56, no. 6, pp. 2775–2781, Dec. 2007.

**YUSHAN LIU** received the B.S. degree in electronic and information engineering from the North University of China, Shanxi, China, where she is currently pursuing the M.S. degree in electronic science and technology. Her research interests include eddy current testing, conductivity classification, and digital signal processing.

**ZHIJIE ZHANG** (Member, IEEE) was born in Taiyuan, Shanxi, China, in 1965. He received the bachelor's degree in automation instrumentation from Tianjin University, the master's degree in testing technology from Taiyuan Mechanical Institute (now the North University of China), in 1989, and the Ph.D. degree in mechanical and electronic engineering from the Department of Mechanical and Electrical Engineering, Beijing Institute of Technology, in 1998.

**WULIANG YIN** (Senior Member, IEEE) received the B.S. and M.S. degrees in electronic measurement and instrumentation from Tianjin University, Tianjin, China, in 1992 and 1995, respectively, and the Ph.D. degree in automotive electronics from Tsinghua University, Beijing, China, in 1999. He is currently a Lecturer with The University of Manchester, U.K. He has authored or coauthored over 100 publications. His current research interests include advanced sensors and instrumentation, automotive electronics, and electromagnetics. He was a recipient of the Science and Technology Award from the Chinese Ministry of Education, in 2000.

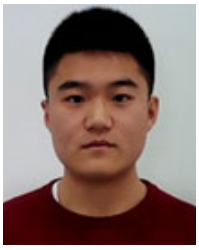

**HAOZE CHEN** was born in Qinhuangdao, Hebei, China, in 1995. He received the bachelor's degree from the North China Institute of Aerospace Engineering, in 2017. He is currently pursuing the Ph.D. degree in instrument science and technology with the School of Instrument and Electronics, North University of China. His research interests include non-destructive testing, signal processing, and machine learning.

**ZHENGHUI YU** was born in Xinzhou, Shanxi, China, in 1997. She received the bachelor's degree in electronic information engineering from the North University of China, where she is currently pursuing the master's degree in instrument science and technology. Her research interest includes composite defect detection.

**QUAN WANG** was born in Meishan, Sichuan, China, in 1995. He received the bachelor's degree in measuring techniques and instruments from Sichuan University of Science and Engineering. He is currently pursuing the master's degree in instrument science and technology with the North University of China. Since 2019, he has been engaged in the research of digital image processing and signal processing.